

A Solution to Lithium Problem by Long-Lived Stau

Joe Sato^{1*}, Takashi Shimomura^{2†}, and Masato Yamanaka^{3‡}

¹*Department of Physics, Saitama University,
Shimo-okubo, Sakura-ku, Saitama, 338-8570, Japan*

²*Faculty of Education, University of Miyazaki,
Miyazaki, 889-2192, Japan*

³*Kobayashi Maskawa Institute, Nagoya University,
Nagoya 464-8602, Japan,
Maskawa Institute, Kyoto Sangyo University,
Kyoto 603-8555, Japan*

Abstract

We review a non-standard Big-Bang Nucleosynthesis (BBN) scenario within the minimal supersymmetric standard model, and propose an idea to solve both ${}^7\text{Li}$ and ${}^6\text{Li}$ problems. Each problem is a discrepancy between the predicted abundance in the standard BBN and observed one. We focus on the stau, a supersymmetric partner of tau lepton, which is a long-lived charged particle when it is the next lightest supersymmetric particle and is degenerate in mass with the lightest supersymmetric particle. The long-lived stau forms a bound state with a nucleus, and provide non-standard nuclear reactions. One of those, the internal conversion process, accelerates the destruction of ${}^7\text{Be}$ and ${}^7\text{Li}$, and leads to a solution to the ${}^7\text{Li}$ problem. On the other hand, the bound state of the stau and ${}^4\text{He}$ enhances productions of n, D, T, and ${}^6\text{Li}$. The over-production of ${}^6\text{Li}$ could solve the ${}^6\text{Li}$ problem. While, the over-productions of D and T could conflict with observations, and the relevant parameter space of the stau is strictly constrained. We therefore need to carefully investigate the stau- ${}^4\text{He}$ bound state to find a condition of solving the ${}^6\text{Li}$ problem. The scenario of the long-lived stau simultaneously and successfully fit the abundances of light elements (D, T, ${}^3\text{He}$, ${}^4\text{He}$, ${}^6\text{Li}$, and ${}^7\text{Li}$) and the neutralino dark matter to the observed ones. Consequently parameter space both of the stau and the neutralino is determined with excellent accuracy.

*E-mail address: joe@phy.saitama-u.ac.jp

†E-mail address: shimomura@cc.miyazaki-u.ac.jp

‡E-mail address: masato.yamanaka@cc.kyoto-su.ac.jp

1 Introduction

Lithium problem is a long standing question[1], which is a discrepancy of the Lithium primordial abundance between observed values and the predicted value by the standard big-bang nucleosynthesis (SBBN). The observed values of ${}^7\text{Li}/\text{H}$ are inferred from metal-poor stars and are set as $(1-2)\times 10^{-10}$, [2, 3, 4, 5, 6, 7] while the theoretical prediction in the SBBN is $(5.24 \pm 0.7) \times 10^{-10}$ [8, 9]. There is discrepancy larger than 4σ level. This is often called ${}^7\text{Li}$ problem.

There is also a tension in ${}^6\text{Li}$ primordial abundance between the observed and the predicted values. The observed value is about 1000 times higher than the predicted one [10], though at this moment it is still controversial [11].

The predictions by the SBBN are given using the standard model (SM) of the particle physics. Though there is still a room for astrophysical explanation of these discrepancies [12], we take it as an evidence which asks us to extend the SM. Since the big-bang nucleosynthesis (BBN) took place from 1 to 1000 sec. after the big bang, it means that we have to add a long-lived particle. Indeed, for example, long-lived massive charged particles induce non-standard nuclear reactions in the BBN, and drastically change light element abundances [13, 14, 15, 16, 17, 18, 19, 20, 21, 22, 23, 24, 25, 26, 27, 28, 29, 30, 31, 32, 33, 34, 35].

The SM has had enormous successes in describing the interactions of the elementary particles, predicting almost every experimental results with accuracy. The recent discovery of the Higgs particle finally crowned the accumulation of successes [36, 37]. However, a number of questions are still left that suggest the presence of a more fundamental theory behind. Among such questions is the nature of dark matter; it became a compelling question during this decade after the precise observations of the universe had reported their results [38, 39]. Though its identity is still unknown, one of the most prominent candidates is weakly interacting massive particles (WIMPs) [40, 41, 42, 43]. As is well known, supersymmetric (SUSY) extensions of the SM provide a stable exotic particle, the lightest supersymmetric particle (LSP), if R parity is conserved. Among LSP candidates, the neutralino LSP is the most suitable for non-baryonic dark matter since its nature fits that of the WIMPs [44, 45]. Neutralinos are a linear combination of neutral fermions which are the supersymmetric partners of hypercharge gauge boson (bino), weak one (wino), and Higgs bosons (higgsinos).

In many scenarios the lightest neutralino LSP, $\tilde{\chi}_1^0$, consists almost of bino. In this case, the next-to-LSP (NLSP) is required to be degenerate in mass to predict the appropriate dark matter density employing coannihilation mechanism [46]. Stau $\tilde{\tau}$, a scalar partner of tau lepton, is the most likely candidate for the NLSP [47]. Their mass difference, $\delta m = m_{\tilde{\tau}} - m_{\tilde{\chi}_1^0}$, must satisfy $\delta m/m_{\tilde{\chi}_1^0} < \text{a few \%}$, where $m_{\tilde{\tau}}$ is the NLSP (stau) mass and $m_{\tilde{\chi}_1^0}$

is the LSP (lightest neutralino) mass. Observed dark matter abundance can be yielded even in $\delta m/m_{\tilde{\chi}_1^0} \simeq 0$. If δm is smaller than tau mass, m_τ , stau cannot decay into 2 body and become very long-lived [48, 49] assuming lepton number conservation. The lifetime can be very long so that the stau can change the SBBN prediction. This stau can effectively destroy ${}^7\text{Be}$ which becomes ${}^7\text{Li}$ by electron capture reaction after the BBN era. Since at the BBN era would-be ${}^7\text{Li}$ exists as ${}^7\text{Be}$, to destruct ${}^7\text{Be}$ effectively means to reduce ${}^7\text{Li}$ primordial abundance. This long-lived stau with the degenerate mass can offer the solution to ${}^7\text{Li}$ problem [22, 26, 50, 33, 51, 52, 53]. We review this idea in this article assuming exact tau number conservation.

In Sec. 2 we introduce the interactions relevant with our scenario and review why the stau is long-lived. Next in Sec. 3 we expound new reactions to the nucleosynthesis chain in the SBBN. Then in Sec. 4 we show numerical results and their interpretation. Finally in Sec. 5 we summarize the scenario and give a brief review when we introduce tiny lepton flavor violation. By introducing it the lithium problems become all clear with sacrifice of adding one parameter.

2 Long-lived stau in stau-neutralino coannihilation scenario

In this section, first, we summarize interactions to formulate decay processes of the stau and non-standard nuclear reactions in the bound states. Then we briefly review a scenario that predicts the long-lived stau, and we calculate the lifetime.

2.1 Interactions

Decay processes of the stau and the non-standard nuclear reactions in a stau-nucleus bound state are described by the following Lagrangian,

$$\begin{aligned} \mathcal{L} = & \tilde{\tau}^* \tilde{\chi}_1^0 (g_L P_L + g_R P_R) \tau + \sqrt{2} G_F \nu_\tau \gamma^\mu P_L \tau J_\mu \\ & + \frac{4G_F}{\sqrt{2}} (\bar{l} \gamma^\mu P_L \nu_l) (\bar{\nu}_\tau \gamma_\mu P_L \tau) + \text{h.c.}, \end{aligned} \quad (1)$$

where $G_F = 1.166 \times 10^{-5} \text{GeV}^{-2}$ is the Fermi coupling constant, $P_{L(R)}$ represents the chiral projection operator, and J_μ represents the weak hadronic current. The effective coupling constants g_L and g_R are given by

$$g_L = \frac{g}{\sqrt{2}} \tan \theta_W \cos \theta_\tau, \quad g_R = -\sqrt{2} g \tan \theta_W \sin \theta_\tau e^{i\gamma_\tau}, \quad (2)$$

where g is the $SU(2)_L$ gauge coupling constant and θ_W is the Weinberg angle. The mass eigenstate of staus is given by the linear combination of $\tilde{\tau}_L$

and $\tilde{\tau}_R$, the superpartners of left-handed and right-handed tau leptons, as

$$\tilde{\tau} = \cos \theta_\tau \tilde{\tau}_L + \sin \theta_\tau e^{-i\gamma_\tau} \tilde{\tau}_R. \quad (3)$$

Here θ_τ is the left-right mixing angle of staus and γ_τ is the CP violating phase.

2.2 Long-lived stau

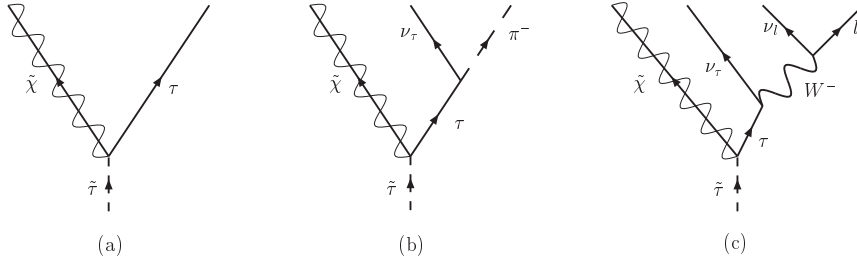


Figure 1: Feynmann diagrams of stau decay: (a) $\tilde{\tau} \rightarrow \tilde{\chi}_1^0 + \tau$, (b) $\tilde{\tau} \rightarrow \tilde{\chi}_1^0 + \nu_\tau + \pi$, (c) $\tilde{\tau} \rightarrow \tilde{\chi}_1^0 + l + \nu_\tau + \nu_l$. Here $l \ni \{e, \mu\}$.

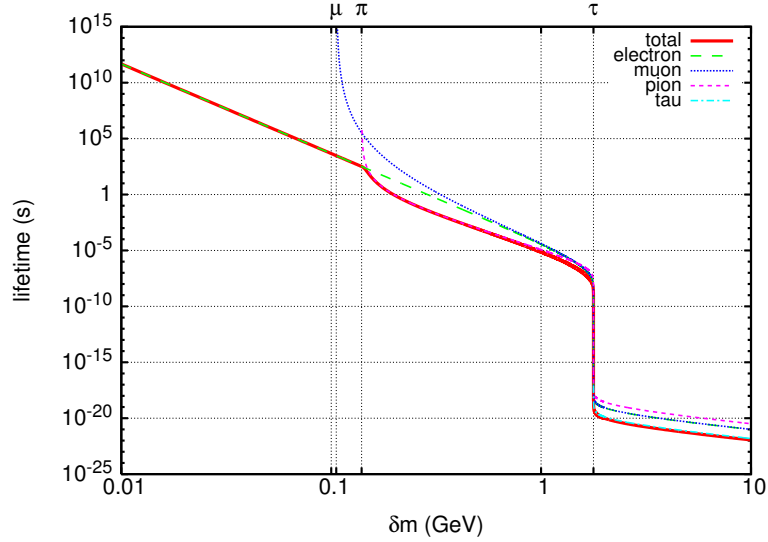


Figure 2: Stau lifetime as a function of $\delta m = m_{\tilde{\tau}} - m_{\tilde{\chi}_1^0}$. We take $m_{\tilde{\tau}} = 300$ GeV, $\theta_\tau = \pi/3$, and $\gamma_\tau = 0$. Each line shows partial lifetimes of each decay channel; $\tilde{\tau} \rightarrow \tilde{\chi}_1^0 + \tau$ (tau), $\tilde{\tau} \rightarrow \tilde{\chi}_1^0 + \nu_\tau + \pi$ (pion), $\tilde{\tau} \rightarrow \tilde{\chi}_1^0 + \nu_\tau + \mu + \bar{\nu}_\mu$ (muon), $\tilde{\tau} \rightarrow \tilde{\chi}_1^0 + \nu_\tau + e + \bar{\nu}_e$ (electron). This figure is taken from Ref. [49].

In the minimal supersymmetric standard model with R-parity conservation, the bino-like neutralino is a WIMP candidate. Direct search results for SUSY particles at the LHC indicate the neutralino with the mass of $m_{\tilde{\chi}_1^0} \gtrsim \mathcal{O}(100 \text{ GeV})$ [54]. Naive calculations of the relic abundance of such the heavy bino-like neutralino dark matter result in an over-closure of the universe. The coannihilation mechanism successfully yields the observed relic abundance of the neutralino dark matter [46, 55, 56]. The key ingredient for the mechanism is the degeneracy in mass between the neutralino dark matter and the NLSP stau, which requires $(m_{\tilde{\tau}} - m_{\tilde{\chi}_1^0})/m_{\tilde{\chi}_1^0} \lesssim \mathcal{O}(\%)$. The degeneracy leads to comparable number densities of them at decoupling of the neutralino dark matter, and makes the effective annihilation rate of the dark matter large through the stau-stau and stau-neutralino annihilation channels. Such a tight degeneracy makes the stau to be long-lived by kinematical suppression in its decay [48, 49]. Especially important and interesting parameter space is wherein the mass difference of the stau and the neutralino, $\delta m = m_{\tilde{\tau}} - m_{\tilde{\chi}_1^0}$, is smaller than tau mass.¹ In such a parameter space the 2-body decay channel (diagram (a) in Fig. 1) closes, and open decay channels are 3- and 4-body ones (diagram (b) and (c) in Fig. 1, respectively).

The stau lifetime is shown by red solid line in Fig. 2. Partial lifetimes of each decay channel are also plotted. The lifetime is drastically enhanced at $\delta m = m_{\tau}$, where the 2-body decay channel closes. Partial widths of 3- and 4-body ones are suppressed by higher order couplings and tight phase space of final states. The dependence of SUSY particle masses on the partial widths is $\Gamma(\tilde{\tau} \rightarrow \tilde{\chi}_1^0 \nu_{\tau} \pi) \propto (\delta m) ((\delta m)^2 - m_{\pi}^2)^{5/2} / m_{\tilde{\tau}}$ and $\Gamma(\tilde{\tau} \rightarrow \tilde{\chi}_1^0 \nu_{\tau} l \bar{\nu}_l) \propto (\delta m)^3 ((\delta m)^2 - m_l^2)^{5/2} / m_{\tilde{\tau}}$. Analytic calculations and more detailed analysis of the partial widths are given in Ref. [49].

The BBN took place from ~ 1 second to ~ 10 minutes after the big bang. Thermally produced stau still exists in the BBN epoch in the parameter region of $\delta m \lesssim 150 \text{ MeV}$, and some of them form a bound state with nuclei by the electromagnetic interaction. In next section, we consider non-standard nuclear reactions in the bound states, and find a solution to the ${}^7\text{Li}$ problem.

3 Non-standard nuclear reactions in stau-nucleus bound state

The long-lived staus form bound states with various nuclei, and the bound states open non-standard nuclear reactions. The internal conversion process is one of the non-standard nuclear reaction, which is analogous to electron

¹ Indeed in large part of parameter space wherein the Higgs mass is consistent with the reported one, the mass difference between the neutralino and the stau is smaller than the mass of tau lepton [57, 58, 52]. Collider phenomenology in such parameter region is extensively studied [59, 60, 61, 62, 63, 64, 65].

capture reaction: $(N \tilde{\tau}^-) \rightarrow \tilde{\chi}_1^0 + \nu_\tau + N'$. Here $(N \tilde{\tau}^-)$ represents a bound state, and $N(N')$ is a nucleus. The internal conversion processes sufficiently destruct ${}^7\text{Be}$ and ${}^7\text{Li}$, and lead to a solution to the ${}^7\text{Li}$ problem (Sec. 3.1). Another non-standard nuclear reaction is spallation processes: $(N \tilde{\tau}^-) \rightarrow \tilde{\chi}_1^0 + \nu_\tau + N' + N'' + \dots$. The spallation processes of ${}^4\text{He}$ could enhance the production of neutron (n), deuteron (D), and triton (T), that leads to a strict bound on properties of the long-lived stau (Sec. 3.2).

3.1 Internal conversion

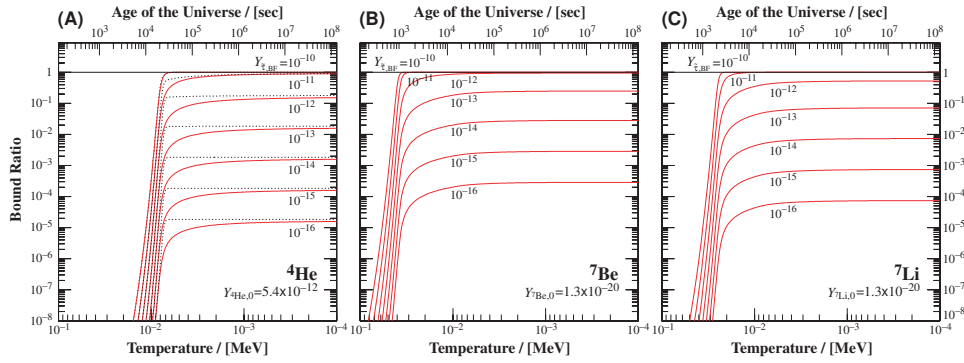


Figure 3: Evolutions of the bound ratio of the nuclei ${}^4\text{He}$, ${}^7\text{Be}$, and ${}^7\text{Li}$ [26]. We vary the abundance of the stau at the time of the formation of the bound state from 10^{-10} to 10^{-16} in each figure. In Fig. 3(A), we also plotted by dotted lines corresponding curves predicted using the Saha equation for reference.

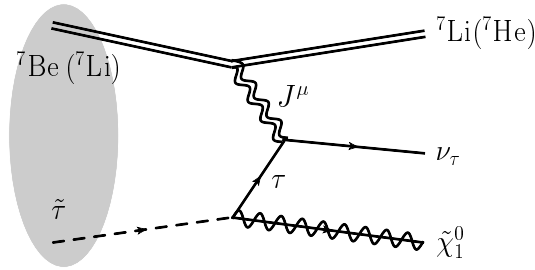


Figure 4: The Feynmann diagrams of internal conversion of ${}^7\text{Be}$ (${}^7\text{Li}$).

In a relatively early stage of the BBN, the long-lived stau forms a bound state with ${}^7\text{Be}$ and ${}^7\text{Li}$ nucleus (Fig. 3). These bound states give rise to the

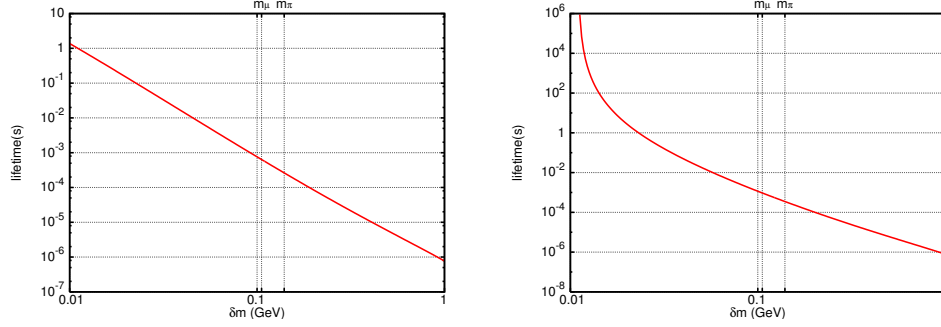


Figure 5: The lifetimes of internal conversion processes as the function of δm [22]. Left panel: $({}^7\text{Be} \tilde{\tau}^-) \rightarrow \tilde{\chi}_1^0 + \nu_\tau + {}^7\text{Li}$, right panel: $({}^7\text{Li} \tilde{\tau}^-) \rightarrow \tilde{\chi}_1^0 + \nu_\tau + {}^7\text{He}$. We take $m_{\tilde{\tau}} = 300\text{GeV}$, $\theta_\tau = \pi/3$, and $\gamma_\tau = 0$ for both reactions.

internal conversion processes (Fig. 4) [22, 19],

$$({}^7\text{Be} \tilde{\tau}^-) \rightarrow \tilde{\chi}_1^0 + \nu_\tau + {}^7\text{Li}, \quad (4a)$$

$$({}^7\text{Li} \tilde{\tau}^-) \rightarrow \tilde{\chi}_1^0 + \nu_\tau + {}^7\text{He}. \quad (4b)$$

The daughter ${}^7\text{Li}$ nucleus in the process (4a) is destructed either by an energetic proton or the process (4b). The daughter ${}^7\text{He}$ nucleus in the process (4b) immediately decays into a ${}^6\text{He}$ nucleus and a neutron. One may consider that ${}^6\text{Li}$ nucleus is produced via beta-decay of this ${}^6\text{He}$, and therefore the internal conversion processes cause the overproduction of ${}^6\text{Li}$.² However, in the parameter region of our interest, ${}^7\text{Li}$ is mainly destructed by a background proton into harmless nuclei. As a result, the bound state formation of ${}^7\text{Li}$ and stau is negligible, and hence we can safely ignore the ${}^6\text{Li}$ production by the process of (4b). Hence the non-standard chain reactions by the long-lived stau could yield smaller ${}^7\text{Be}$ and ${}^7\text{Li}$ abundances than those in the standard BBN scenario, that is the requirement for solving the ${}^7\text{Li}$ problem (see Introduction). This is the scenario we proposed.

The reaction rate of the internal conversion processes is given by

$$\Gamma_{\text{IC}} = |\psi|^2 \cdot (\sigma v)_{\text{IC}}. \quad (5)$$

The front part in the right-hand side expresses overlap of wave functions in an initial state. We assume that the bound state is in the S state of a hydrogen-like atom, and obtain the overlap as $|\psi|^2 = 1/(\pi a_{\text{nucl}}^3)$. Here $a_{\text{nucl}} = (1.2 \times A^{1/3}) \text{fm}$ is the radius of a nucleus and A is its mass number.

²This ${}^6\text{Li}$ production process is different process from the catalyzed fusion of ${}^4\text{He} + \text{D}$ that Pospelov pointed out in Ref. [14].

The remaining part in the right-hand side expresses the cross section of elementary process. For the process $({}^7\text{Be } \tilde{\tau}^-) \rightarrow \tilde{\chi}_1^0 + \nu_\tau + {}^7\text{Li}$,

$$(\sigma v)_{\text{IC}} = \frac{1}{(2E_{\tilde{\tau}})(2E_{\text{Be}})} \int \frac{d^3\mathbf{p}_\nu}{(2\pi)^3 2E_\nu} \frac{d^3\mathbf{p}_{\tilde{\chi}}}{(2\pi)^3 2E_{\tilde{\chi}}} \frac{d^3\mathbf{p}_{\text{Li}}}{(2\pi)^3 2E_{\text{Li}}} \quad (6)$$

$$\times |\mathcal{M}({}^7\text{Be } \tilde{\tau}^- \rightarrow \tilde{\chi}_1^0 \nu_\tau {}^7\text{Li})|^2 (2\pi)^4 \delta^{(4)}(p_{\tilde{\tau}} + p_{\text{Be}} - p_{\tilde{\chi}} - p_\nu - p_{\text{Li}}).$$

Here p_i and E_i are the momentum and the energy of a particle species i , respectively. The amplitude is decomposed into leptonic and hadronic part as

$$\mathcal{M}({}^7\text{Be } \tilde{\tau}^- \rightarrow \tilde{\chi}_1^0 \nu_\tau {}^7\text{Li}) = \langle {}^7\text{Li} | J^\mu | {}^7\text{Be} \rangle \langle \tilde{\chi}_1^0 \nu_\tau | j_\mu | \tilde{\tau} \rangle. \quad (7)$$

The leptonic part is straightforwardly calculated. The matrix element of the nuclear conversion is evaluated by the ft value obtained from β decay experiments. The experimental ft value is available for ${}^7\text{Li} \leftrightarrow {}^7\text{Be}$ but not for ${}^7\text{Li} \leftrightarrow {}^7\text{He}$. We assume that the two processes (4) have the same ft value. As long as we consider the quantum numbers of the ground state of ${}^7\text{Li}$ and ${}^7\text{He}$, it is reasonable to expect a Gamow-Teller transition can occur since they are similar with those of ${}^6\text{He}$ and ${}^6\text{Li}$ and we know that they make a Gamow-Teller transition. The Gamow-Teller transition is superallowed and has a similar ft value to the Fermi transition such as ${}^7\text{Li} \leftrightarrow {}^7\text{Be}$.

The time scale of the internal conversion processes, (4a) and (4b), are shown in Fig. 5 as a function of δm . The time scale of $({}^7\text{Li } \tilde{\tau}^-) \rightarrow \tilde{\chi}_1^0 + \nu_\tau + {}^7\text{He}$ diverges around $\delta m = m_{\tau_{\text{He}}} - m_{\tau_{\text{Li}}} = 11.7 \text{ MeV}$, below which the internal conversion is kinematically forbidden.

We find that the reaction time scale is in the order of 10^{-3} sec. Thus, compared with a typical time scale at the BBN epoch, a parent nucleus is converted into another nucleus in no time once the bound state is formed. The bound state formation makes the interaction between the stau and a nucleus more efficiently by two reasons: (i) the overlap of the wave functions of the stau and a nucleus becomes large since these are confined in the small space, (ii) the short distance between the stau and a nucleus allows virtual exchange of the hadronic current even if $\delta m < m_\pi$.

It is important to emphasize that the internal conversion processes can be activated only in the neutralino LSP scenarios, but not in the gravitino LSP scenarios. A key difference between these scenarios is the origin of longevity of the stau. In the neutralino LSP scenarios, the longevity is ensured by tight phase space suppression in its decay. Dominant channels of the particle decay of the stau are 3- and 4-body final state processes. The internal conversion processes are also 3-body final state processes since the processes occur via off-shell hadronic current exchange in the bound state, but the initial states are 2-body system, i.e., the stau and a nucleus. Consequently, compared with the particle decay of the stau, the phase space suppression is relaxed, and hence the time scale becomes much shorter than

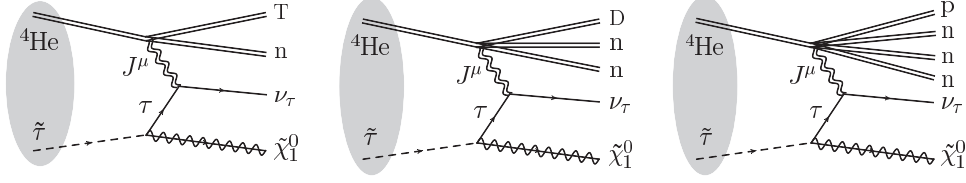


Figure 6: ${}^4\text{He}$ spallation processes.

the stau lifetime. On the other hand, in the gravitino LSP scenarios, the longevity is ensured by the Planck suppressed interaction in its decay. Dominant decay channel is the 2-body one, $\tilde{\tau} \rightarrow \tilde{G}\tau$. In this scenario, even in the bound state, the 2-body decay process dominates over the internal conversion processes, because the internal conversion needs the hadronic current which is suppressed by the Fermi couplings. Thus the internal conversion processes in the gravitino LSP scenario can not be activated.

3.2 Spallation reactions and stau catalyzed fusion

There exists two types of non-standard reactions for the bound state of a stau and a ${}^4\text{He}$ nucleus:

(1) stau-catalyzed fusion

$$({}^4\text{He} \tilde{\tau}^-) + \text{D} \rightarrow \tilde{\tau} + {}^6\text{Li}, \quad (8)$$

(2) spallation of the ${}^4\text{He}$ nucleus

$$({}^4\text{He} \tilde{\tau}^-) \rightarrow \tilde{\chi}_1^0 + \nu_\tau + \text{T} + \text{n}, \quad (9\text{a})$$

$$({}^4\text{He} \tilde{\tau}^-) \rightarrow \tilde{\chi}_1^0 + \nu_\tau + \text{D} + \text{n} + \text{n}, \quad (9\text{b})$$

$$({}^4\text{He} \tilde{\tau}^-) \rightarrow \tilde{\chi}_1^0 + \nu_\tau + \text{p} + \text{n} + \text{n} + \text{n}. \quad (9\text{c})$$

Since the origin of longevity of the stau determines which light element is over-produced by these non-standard reactions, we need to carefully and independently study the evolution of the stau- ${}^4\text{He}$ bound state in each scenario that possesses the origins of the longevity different from each other.

The catalyzed fusion process enhances the ${}^6\text{Li}$ production [14]. The catalyzed fusion process is a type of photon-less nuclear transfer reaction, and typical rate of such a reaction is formulated by using the astrophysical S-factor as $S(0) \sim 10^2 \text{ keV b}$ [66]. Thermal averaged cross section of the catalyzed fusion is precisely calculated in Refs. [21, 28], which is much larger than that of the ${}^6\text{Li}$ production in the SBBN, ${}^4\text{He} + \text{D} \rightarrow {}^6\text{Li} + \gamma$, by 6-7 orders of magnitude. In the SBBN, since the ${}^6\text{Li}$ production ${}^4\text{He} + \text{D} \rightarrow {}^6\text{Li} + \gamma$ is an E1 forbidden transition reaction, the reaction rate is tiny and the magnitude is given by the astrophysical S-factor as $S(0) \sim 2 \times 10^{-6} \text{ keV b}$ [66]. The over-production of ${}^6\text{Li}$ nucleus by the catalyzed fusion process leads to stringent

constraints both on the lifetime and the number density of the long-lived charged particles in the BBN epoch. [14].

Reaction (9) is essentially a spallation of the ${}^4\text{He}$ nucleus, producing a triton, a deuteron, and neutrons. We formulate the reaction rate of a spallation process $({}^4\text{He } \tilde{\tau}^-) \rightarrow \tilde{\chi}_1^0 + \nu_\tau + \text{T} + \text{n}$. The reaction rate is given as

$$\Gamma(({}^4\text{He } \tilde{\tau}^-) \rightarrow \tilde{\chi}_1^0 + \nu_\tau + \text{T} + \text{n}) = |\psi|^2 \cdot \sigma v_{\text{Tn}}. \quad (10)$$

With the same formulation in the case of internal conversion process, the overlap of wave functions of the stau and the ${}^4\text{He}$ nucleus is calculated as $|\psi|^2 = (Z\alpha m_{\text{He}})^3/\pi$ where Z is the atomic number of nucleus and α is the fine structure constant. The cross section $\sigma v_{\text{Tn}} \equiv \sigma v(({}^4\text{He } \tilde{\tau}^-) \rightarrow \tilde{\chi}_1^0 \nu_\tau \text{Tn})$ is calculated as follows,

$$\begin{aligned} \sigma v_{\text{Tn}} = & \frac{1}{2E_{\tilde{\tau}}} \int \frac{d^3\mathbf{p}_\nu}{(2\pi)^3 2E_\nu} \frac{d^3\mathbf{p}_{\tilde{\chi}}}{(2\pi)^3 2E_{\tilde{\chi}}} \frac{d^3\mathbf{q}_{\text{n}}}{(2\pi)^3} \frac{d^3\mathbf{q}_{\text{T}}}{(2\pi)^3} |\mathcal{M}(({}^4\text{He } \tilde{\tau}^-) \rightarrow \tilde{\chi}_1^0 \nu_\tau \text{Tn})|^2 \\ & \times (2\pi)^4 \delta^{(4)}(p_{\tilde{\tau}} + p_{\text{He}} - p_\nu - q_{\text{T}} - q_{\text{n}}). \end{aligned} \quad (11)$$

The amplitude is decomposed into leptonic and hadronic part as

$$\mathcal{M}(({}^4\text{He } \tilde{\tau}^-) \rightarrow \tilde{\chi}_1^0 \nu_\tau \text{Tn}) = \langle \text{Tn} | J^\mu | {}^4\text{He} \rangle \langle \tilde{\chi}_1^0 \nu_\tau | j_\mu | \tilde{\tau} \rangle. \quad (12)$$

The hadronic current J^μ is given by a vector current V_μ and an axial vector current A_μ as $J_\mu = V_\mu + g_A A_\mu$, where g_A is the axial coupling constant. The relevant components are V^0 and A^i ($i = 1, 2, 3$). We take these operators as a sum of single-nucleon operators as

$$V^0 = \sum_{a=1}^4 \tau_a^- e^{i\mathbf{q} \cdot \mathbf{r}_a}, \quad A^i = \sum_{a=1}^4 \tau_a^- \sigma_a^i e^{i\mathbf{q} \cdot \mathbf{r}_a}, \quad (13)$$

where \mathbf{q} is the momentum carried by the current, \mathbf{r}_a are the spatial coordinates of the a -th nucleon ($a \in \{1, 2, 3, 4\}$), and τ_a^- and σ_a^i denote the isospin ladder operators and the spin operators of the a -th nucleon, respectively. Each component leads to a part of hadronic matrix element:

$$\langle \text{Tn} | V^0 | {}^4\text{He} \rangle = \langle \text{Tn} | A^+ | {}^4\text{He} \rangle = -\langle \text{Tn} | A^- | {}^4\text{He} \rangle = -\langle \text{Tn} | A^3 | {}^4\text{He} \rangle = \sqrt{2} \mathcal{M}_{\text{Tn}}, \quad (14)$$

where $A^\pm = (A^1 \pm iA^2)/\sqrt{2}$. We need wave functions of ${}^4\text{He}$, T, and n to calculate the hadronic amplitude. The formulation and explicit formulae of the wave functions are given in Appendix A in Ref. [33]. Consequently we obtain the hadronic matrix element as follows,

$$\begin{aligned} \mathcal{M}_{\text{Tn}} = & \left(\frac{128\pi}{3} \frac{a_{\text{He}} a_{\text{T}}^2}{(a_{\text{He}} + a_{\text{T}})^4} \right)^{3/4} \\ & \times \left\{ \exp\left[-\frac{\mathbf{q}_{\text{T}}^2}{3a_{\text{He}}}\right] - \exp\left[-\frac{\mathbf{q}_{\text{n}}^2}{3a_{\text{He}}} - \frac{(\mathbf{q}_{\text{T}} + \mathbf{q}_{\text{n}})^2}{6(a_{\text{He}} + a_{\text{T}})}\right] \right\}. \end{aligned} \quad (15)$$

Table 1: Input values of the matter radius R_{mat} for D, T, and ^4He , the magnetic radius R_{mag} for p and n, nucleus mass m_X , excess energy Δ_X for the nucleus X , and each reference.

nucleus	$R_{\text{mat(mag)}} [\text{fm}]/[\text{GeV}^{-1}]$	$m_X [\text{GeV}]$	$\Delta_X [\text{GeV}]$
p	0.876 / 4.439 [67]	0.9383 [68]	6.778×10^{-3} [69]
n	0.873 / 4.424 [70]	0.9396 [68]	8.071×10^{-3} [69]
D	1.966 / 9.962 [71]	1.876 [69]	1.314×10^{-2} [69]
T	1.928 / 9.770 [72]	2.809 [69]	1.495×10^{-2} [69]
^4He	1.49 / 7.55 [73]	3.728 [69]	2.425×10^{-3} [69]

Here \mathbf{q}_T and \mathbf{q}_n are three-momenta of the triton and the neutron, respectively, and a_{He} and a_T are related to the mean square matter radius R_{mat} by $a_{\text{He}} = 9/(16(R_{\text{mat}})_{\text{He}}^2)$ and $a_T = 1/(2(R_{\text{mat}})_T^2)$, respectively. We list in Table 1 input values of the matter radius. The leptonic part is straightforwardly calculated to be

$$\begin{aligned} |\langle \tilde{\chi}_1^0 \nu_\tau | j_0 | \tilde{\tau} \rangle|^2 &= |\langle \tilde{\chi}_1^0 \nu_\tau | j_z | \tilde{\tau} \rangle|^2 = 4G_F^2 |g_R|^2 \frac{m_{\tilde{\chi}_1^0} E_\nu}{m_\tau^2}, \\ |\langle \tilde{\chi}_1^0 \nu_\tau | j_\pm | \tilde{\tau} \rangle|^2 &= 4G_F^2 |g_R|^2 \frac{m_{\tilde{\chi}_1^0} E_\nu}{m_\tau^2} \left(1 \mp \frac{p_\nu^z}{E_\nu} \right), \end{aligned} \quad (16)$$

where E_ν and p_ν^z are the energy and the z -component of the momentum of the tau neutrino, respectively. Consequently we obtain the cross section as follows,

$$\sigma v_{Tn} = \frac{8}{\pi^2} \left(\frac{32}{3\pi} \right)^{3/2} g^2 \tan^2 \theta_W \sin^2 \theta_\tau (1 + 3g_A^2) G_F^2 \Delta_{Tn}^4 \frac{m_T m_n}{m_{\tilde{\tau}} m_\tau^2} \frac{a_{\text{He}}^{3/2} a_T^3}{(a_{\text{He}} + a_T)^5} I_{Tn}, \quad (17)$$

where I_{Tn} is a dimensionless integral, which includes kinematical information of the reaction. The numerical result of I_{Tn} is plotted in Fig. 7, and the analytical formula is given by Eq. (17) in Ref. [33]. Here Δ_{Tn} , k_T , and k_n are defined as $\Delta_{Tn} \equiv \delta m + \Delta_{\text{He}} - \Delta_T - \Delta_n - E_b$, $k_T \equiv \sqrt{2m_T \Delta_{Tn}}$, and $k_n \equiv \sqrt{2m_n \Delta_{Tn}}$. Here Δ_X is the excess energy of the nucleus X , and E_b is the binding energy of ($^4\text{He} \tilde{\tau}^-$) system.

We compare the rate of the spallation and that of the stau-catalyzed fusion. We first note that the rate of stau-catalyzed fusion strongly depends on the temperature [21], and we fix the reference temperature to be 30 keV. Staus begin to form a bound state with ^4He at this temperature, which corresponds to cosmic time of 10^3 s. Thus the bound state is formed when the lifetime of the staus is longer than 10^3 s.

Figure 8 shows the timescale of the spallation processes as a function of δm . The lifetime of free stau is plotted by a solid line. We took the reference values of $m_{\tilde{\tau}} = 350 \text{ GeV}$, $\sin \theta_\tau = 0.8$, and $\gamma_\tau = 0$. The timescale of

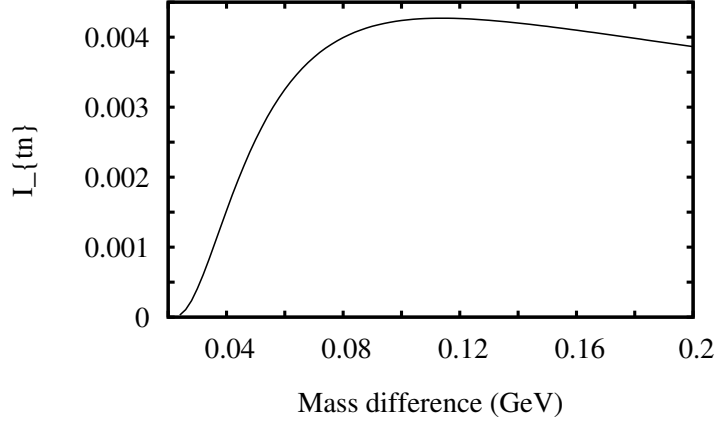


Figure 7: Numerical result of I_{Tn} as a function of $\delta m = m_{\tilde{\tau}} - m_{\tilde{\chi}_1^0}$ for $m_{\tilde{\tau}} = 350\text{GeV}$.

the stau-catalyzed fusion at the temperature of 30 keV is also shown by the horizontal dashed line. Once a bound state is formed, as long as the phase space of spallation processes are open sufficiently that is $\delta m \gtrsim 0.026\text{ GeV}$, those processes dominate over other processes. There $\tilde{\tau}$ property is constrained to evade the over-production of D and/or T. For $\delta m \lesssim 0.026\text{ GeV}$, the dominant process of $({}^4\text{He } \tilde{\tau}^-)$ is stau-catalyzed fusion, since the free $\tilde{\tau}$ lifetime is longer than the timescale of stau-catalyzed fusion. Thus light gray region is forbidden due to the over-production of ${}^6\text{Li}$.

The result of Fig.8 is not much altered by varying the parameters relevant with $\tilde{\tau}$. First the cross sections of the spallation processes are inversely proportional to $m_{\tilde{\tau}}$, and then the timescale of each process linearly increases as $m_{\tilde{\tau}}$ increases. Thus, even when $m_{\tilde{\tau}}$ is larger than $m_{\tilde{\tau}} = 350\text{ GeV}$ by up to a factor of ten, the region of ${}^6\text{Li}$ over-production scarcely changes. Next we point out that our result depends only mildly on the left-right mixing of the stau. Indeed, the cross section of the ${}^4\text{He}$ spallation is proportional to $\sin^2 \theta_\tau$. The order of its magnitude will not change as long as the right-handed component is significant.

4 Numerical Results

In this section, we show numerical results of the number density and the allowed parameter region of the stau by solving the Boltzmann equations at BBN era. Details of numerical calculations are explained in Ref. [26].

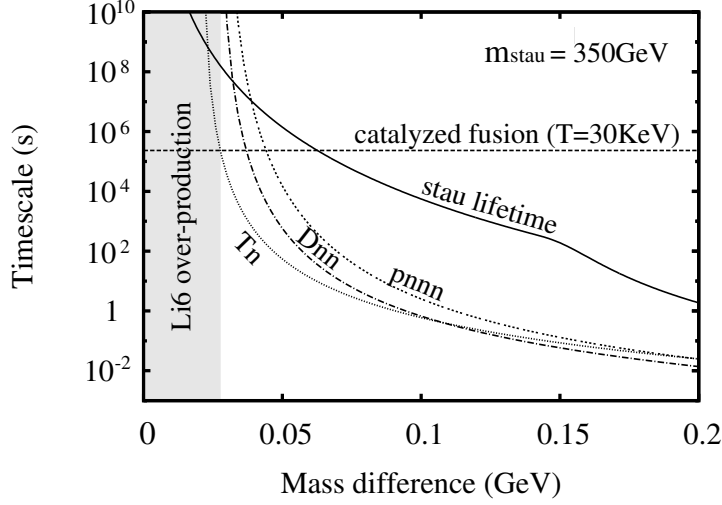


Figure 8: Timescale of spallation processes as a function of δm [33] and the stau-catalyzed fusion at the universe temperature $T = 30 \text{ keV}$ [21]. The lifetime of free $\tilde{\tau}$ (solid line) is also depicted. Here we took $m_{\tilde{\tau}} = 350 \text{ GeV}$, $\sin \theta_{\tau} = 0.8$, and $\gamma_{\tau} = 0$.

4.1 Stau Number Density

The neutralino LSP is the dark matter in our scenario, hence its abundance must coincide with the observed dark matter abundance at the present time. Most of the neutralino LSP is produced via decays of the long-lived stau during the BBN. Thus, before the BBN starts, the total abundance of stau and the neutralino LSP must be the same as that of the dark matter.

We show the total abundance of the staus and the neutralino LSP in terms of left-right mixing parameter. In the left panel of Fig. 9, each curve corresponds to the stau mass 300, 350 and 400 GeV, respectively, and horizontal (yellow) band and the dotted lines represent the allowed region from the WMAP observation at the 3σ level ($0.0913 \leq \Omega_{DM} h^2 \leq 0.1285$) and at the 2σ level ($0.0963 \leq \Omega_{DM} h^2 \leq 0.1213$) [74]. The left-side region from the vertical lines in the figure, corresponding to $m_{\tilde{\tau}} = 400, 350, 300 \text{ GeV}$ from left to right, represents the left-handed sneutrino LSP. The left-handed sneutrino dark matter has been ruled out by constraints from the direct detection experiments [75] and therefore only the right-side region is allowed. Here we took $\gamma_{\tau} = 0$ and $\delta m = 100 \text{ MeV}$.

We can see that the total abundance increases first as the heavier stau mixes to the lighter stau, then turns to decrease at $\sin \theta_{\tau} \simeq 0.8$. The increase of the abundance can be understood by the fact that the annihilation cross section of $\tilde{\tau} + \tilde{\tau} \rightarrow \tau + \tau$, $\tilde{\tau}^* + \tilde{\tau}^* \rightarrow \bar{\tau} + \bar{\tau}$ and $\tilde{\tau} + \tilde{\tau}^* \rightarrow \tau + \bar{\tau}$ becomes smaller as the heavier stau mixes. The increase is gradually compensated

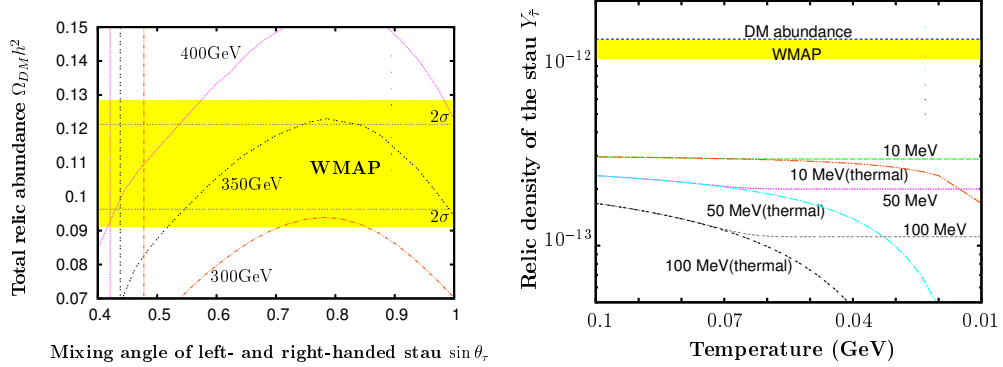


Figure 9: Left: Total abundance of staus and neutralinos [50]. Right: The evolution of the number density of negative charged stau [50].

by two annihilation processes, $\tilde{\tau} + \tilde{\tau}^* \rightarrow W^+ + W^-$ and $\tilde{\chi}_1^0 + \tilde{\tau} \rightarrow W^- + \nu_\tau$, as the left-right mixing becomes large. Here $\tilde{\tau}^*$ denotes anti-particle of stau. The latter process can not be ignored because left-handed sneutrino is degenerate to stau and neutralino in the present parameter set. These processes become significant for $\sin \theta_\tau < 0.8$. Another process which reduces the total abundance due to the left-right mixing is $\tilde{\tau} + \tilde{\tau}^* \rightarrow t + \bar{t}$ through s-channel exchange of the heavy Higgses. This annihilation process becomes significant as the mixing reaches to $\pi/4$ and the masses of two staus are split. In the left panel, the mass difference between the lighter and the heavier stau is fixed to be 30 GeV to maximize the dark matter abundance, but the same result can be obtained by changing the stau mass for another values of the mass difference. As is seen, the total abundance also strongly depends on $m_{\tilde{\tau}}$. This is understood as follows. In the non-relativistic limit, since the relic number density of relic species is proportional to $(m_{relic} \langle \sigma v \rangle_{\text{sum}})^{-1}$ and $\langle \sigma v \rangle_{\text{sum}}$ is proportional to $1/m_{relic}^2$ [76], the total number density N is proportional to $m_{\tilde{\tau}}$,

$$N \propto \frac{1}{m_{\tilde{\tau}} \langle \sigma v \rangle_{\text{sum}}} \propto \frac{1}{1/m_{\tilde{\tau}}} = m_{\tilde{\tau}}, \quad (18)$$

and the total abundance is given by $\Omega_{DM} h^2 \sim m_{\tilde{\tau}} N$. Thus the total abundance is proportional to $m_{\tilde{\tau}}^2$, and it is consistent with the result in Fig. 9.

The right panel of Fig. 9 shows the evolution of the number density of stau as a function of the universe temperature. Here we took $m_{\tilde{\tau}} = 350$ GeV, $\sin \theta_\tau = 0.8$, and $\gamma_\tau = 0$ and chose $\delta m = 10$ MeV, 50 MeV, and 100 MeV as sample points. Each line with attached $[\delta m]$ shows the number density of stau, while the one with attached $[\delta m(\text{thermal})]$ shows the equilibrium one. Horizontal dotted line represents the relic density of dark matter, which is

the total abundance and used as an initial condition of total value for the number density ratio. Yellow band represents the allowed region from the WMAP observation at the 2σ level [74].

The number density evolution of stau is qualitatively understood as follows. As shown in the figure, the freeze-out temperature of stau is almost independent of δm . It is determined by the exchange processes, $\tilde{\tau}\tau^+ \leftrightarrow \tilde{\chi}_1^0\gamma$ and $\tilde{\tau}\gamma \leftrightarrow \tilde{\chi}_1^0\tau^-$, whose magnitude $\langle\sigma v\rangle Y_{\tilde{\tau}} Y_{\gamma}$ is governed by the factor $e^{-(m_{\tau}-\delta m)/T}$, where m_{τ} represents the tau lepton mass. The freeze-out temperature of the stau density $T_{f(\text{ratio})}$ is given by $(m_{\tau}-\delta m)/T_{f(\text{ratio})} \simeq 25$, since the cross section of the exchange process is of the same magnitude as weak processes. Thus $T_{f(\text{ratio})}$ hardly depends on δm . In contrast, the ratio of the number density between stau and neutralino depends on δm , $n_{\tilde{\tau}}/n_{\tilde{\chi}} \sim \exp(-\delta m/T)$, since they follow the Boltzmann distribution before their freeze-out. Thus, the relic density of stau strongly depends on δm .

Here, we comment on the dependence of the stau relic density $n_{\tilde{\tau}-}$ on other parameters such as $m_{\tilde{\tau}}$, θ_{τ} , and γ_{τ} . The number density of the negatively charged stau is expressed in terms of the total relic density N by

$$n_{\tilde{\tau}-} = \frac{N}{2(1 + e^{\delta m/T_{f(\text{ratio})}})} . \quad (19)$$

Here, the freeze-out temperature $T_{f(\text{ratio})}$ hardly depends on these parameters. This is because the cross section of the exchange processes are changed by these parameters at most by factors but not by orders of magnitudes, and the $T_{f(\text{ratio})}$ depends logarithmically on $\langle\sigma v\rangle$ [76, 50]. On the other hand, the total relic density N is proportional to $m_{\tilde{\tau}}$ as in Eq. (18). The value of N is also affected by the left-right mixing θ_{τ} as seen in Fig. 9 since the annihilation cross section depends on this parameter. In contrast, γ_{τ} scarcely affects the relic density, since this parameter appears in the annihilation cross section through the cross terms of the contributions from the left-handed stau and the right-handed one, and such terms are always accompanied by the suppression factor of $m_{\tau}/m_{\tilde{\tau}}$ compared to the leading contribution. Thus the relic number density of stau $n_{\tilde{\tau}}$ strongly depends on $m_{\tilde{\tau}}$ and θ_{τ} while scarcely depends on γ_{τ} .

After the number density of stau freezes out, stau decays according to its lifetime [49], or forms a bound state with a nucleus in the BBN era. Their formation rate has been studied in literatures [15, 22, 19]. The bound states modify the predictions of SBBN, and make it possible to solve the ${}^7\text{Li}$ problem via internal conversion processes in the bound state [22, 19, 26].

4.2 Parameter region for the solution of ${}^7\text{Li}$ Problem

Next, we show the allowed regions of the parameter space in which the ${}^7\text{Li}$ problem can be solved. We include in our analyses not only the internal con-

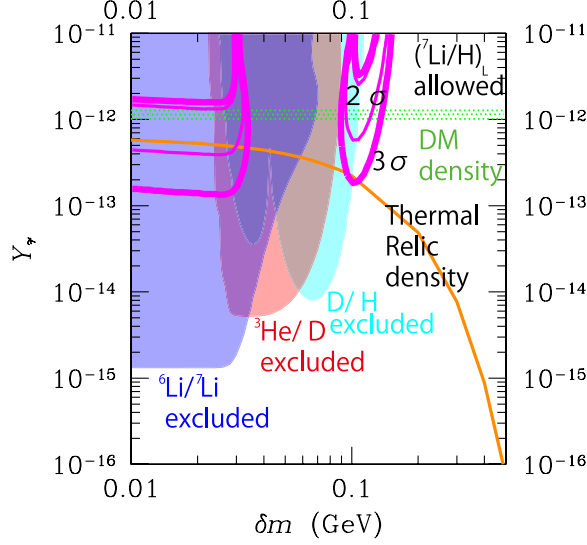


Figure 10: Allowed regions from observational light element abundances at 2σ [33]. The higher value of the observational ${}^7\text{Li}/\text{H}$ in [2] denoted by $({}^7\text{Li}/\text{H})_{\text{H}}$ are adopted. Thin and thick lines represent the 2σ and 3σ only for ${}^7\text{Li}/\text{H}$, respectively. The horizontal band means the observationally-allowed dark matter density. The parameters are taken as $m_{\tilde{\tau}} = 350$ GeV, $\sin\theta_{\tau} = 0.8$, and $\gamma_{\tau} = 0$.

version processes but also ${}^4\text{He}$ spallation processes and $\tilde{\tau}$ catalyzed nuclear fusion explained in the previous section.

As mentioned in the introduction, the ${}^7\text{Li}$ problem is a discrepancy between the theoretical value of ${}^7\text{Li}$ abundance predicted in the SBBN and the observational one. The prediction of the SBBN for the ${}^7\text{Li}$ to H ratio is ${}^7\text{Li}/\text{H} = 4.47^{+0.58}_{-0.66} \times 10^{-10}$ for baryon to photon ratio $\eta = (6.225 \pm 0.170) \times 10^{-10}$ (68% C.L.) by the WMAP [77]. On the other hand, the primordial ${}^7\text{Li}$ abundance is observed in metal-poor halo stars as absorption lines [1]. Observationally-inferred values of the primordial ${}^7\text{Li}$ to H ratio is ${}^7\text{Li}/\text{H} = 2.34^{+0.30}_{-0.35} \times 10^{-10}$ for a high value[2]. (See also Refs. [78, 10, 79, 3] for another values.) Therefore the discrepancy remains more than 3σ between theoretical and observational values.

In Fig. 10, we plot the allowed parameter region in δm and $Y_{\tilde{\tau}}$ plane, which is obtained by comparing the theoretical values to observational ones for the high value of ${}^7\text{Li}/\text{H}$. The parameters for the stau are taken to be $m_{\tilde{\tau}} = 350$ GeV, $\sin\theta_{\tau} = 0.8$, and $\gamma_{\tau} = 0$. We have adopted following another observational constraints on the light element abundances: an upper bound on the ${}^6\text{Li}$ to ${}^7\text{Li}$ ratio, ${}^6\text{Li}/{}^7\text{Li} < 0.046 + 0.022$ [10], the deuteron to

hydrogen ratio, $D/H = (2.80 \pm 0.20) \times 10^{-5}$ [80], and an upper bound on the ${}^3\text{He}$ to D ratio, ${}^3\text{He}/D < 0.87 + 0.27$ [81]. The solid (orange) line denotes a theoretical value of the thermal relic abundance for the stau [50] while keeping observed dark matter density at $\Omega_{\text{DM}} h^2 = 0.11 \pm 0.01$ (2σ) [77] as total $\tilde{\chi}_1^0 + \tilde{\tau}$ abundance. For reference, we also plot the observationally-allowed dark matter density in the figures by a horizontal band.

At around $\delta m \sim 0.1$ GeV, we found that there is an allowed region at $Y_{\tilde{\tau}} \sim 10^{-13}$ for $\delta m \sim 130$ MeV to solve the ${}^7\text{Li}$ problem at 3σ . It is shown that ${}^7\text{Li}/H$ can be fitted to the observational value without conflicting with the other light element abundances.³ As shown in Fig. 10, it is impressive that the relic density is consistent with the allowed region at $Y_{\tilde{\tau}} = 2 \times 10^{-13}$ at 3σ in case of the high value of ${}^7\text{Li}/H$. On the other hand, since the stau lifetime is longer than the formation timescale of the stau- ${}^4\text{He}$ bound state in the region $\delta m \lesssim 100$ MeV, over-productions of D and ${}^3\text{He}$ by the ${}^4\text{He}$ spallation processes exclude the region $30 \text{ MeV} \lesssim \delta m \lesssim 100 \text{ MeV}$ and $Y_{\tilde{\tau}} \gtrsim 10^{-14}$. In the smaller δm region, the ${}^4\text{He}$ spallation processes kinematically close, and the catalyzed fusion is activated. Consequently, the observational ${}^6\text{Li}/{}^7\text{Li}$ ratio excludes the region where $Y_{\tilde{\tau}} \gtrsim 10^{-15}$ and $\delta m \lesssim 100$ MeV. This feature is explained as follows.

We have adopted following observational abundances of ${}^6\text{Li}$ and ${}^7\text{Li}$. Throughout this subsection, n_i denotes the number density of a particle “ i ”, and observational errors are given at 1σ . For the $n_{{}^6\text{Li}}$ to $n_{{}^7\text{Li}}$ ratio, we use the upper bound [10],

$$(n_{{}^6\text{Li}}/n_{{}^7\text{Li}})_p < 0.046 \pm 0.022 + 0.106, \quad (20)$$

with a conservative systematic error (+0.106) [86], while the ${}^7\text{Li}$ abundance is given above. In the current scenario ${}^6\text{Li}$ can be overproduced by the catalyzed fusion (8). The abundance of ${}^6\text{Li}$ through this process is approximately represented by

$$\Delta Y_{{}^6\text{Li}} \sim \frac{\langle \sigma v \rangle_{{}^6\text{Li}} n_{\text{D}}}{H} Y_{\tilde{\tau}-}, \quad (21)$$

with $\langle \sigma v \rangle_{{}^6\text{Li}}$ the thermal average of the cross section times the relative velocity for this process [21], and n_{D} the number density of deuterium. Note that in Eq.(21), it is roughly assumed that all staus have been bound to ${}^4\text{He}$ when the ${}^6\text{Li}$ production proceeds via the reaction (8). By using (20), we see that the additional ${}^6\text{Li}$ production is constrained to be $\Delta Y_{{}^6\text{Li}} < \mathcal{O}(10^{-21})$. Numerical value of $\langle \sigma v \rangle_{{}^6\text{Li}}$ gives $\langle \sigma v \rangle_{{}^6\text{Li}} n_{\text{D}}/H \sim \mathcal{O}(10^{-6})$ at $T \sim 10$ keV. Then from (21) it is found that the upper bound on the abundance of stau should be $Y_{\tilde{\tau}-} \lesssim 10^{-15}$. Because the bound state (${}^4\text{He} \tilde{\tau}^-$) forms at $T \lesssim 10$ keV, this process is strongly constrained for $\tau_{\tilde{\tau}-} \gtrsim 10^4$ s with $\tau_{\tilde{\tau}-}$ being the stau lifetime, which corresponds to $\delta m \lesssim 100$ MeV. Note that the ratio

³See also [82, 19, 83, 84, 85] for another mechanisms to reduce ${}^7\text{Li}/H$.

$\langle\sigma v\rangle_{^6\text{Li}n_{\text{D}}}/H$ rapidly decreases as the cosmic temperature decreases, and this late production of ^6Li is much more effective just after formation of the bound state. This is the reason why we can estimate (21) at around 10 keV.

On the other hand, the rates of ^7Be and ^7Li destruction through the internal conversion [22, 19, 26] could be nearly equal to the formation rates of the bound state ($^7\text{Be}\tilde{\tau}^-$) and ($^7\text{Li}\tilde{\tau}^-$), respectively. This is because the timescale of the destruction through the internal conversion is much faster than that of any other nuclear reaction rates and the Hubble expansion rate. Then the amount of destroyed ^7Be (or ^7Li after its electron capture) is approximately represented by

$$\Delta Y_{^7\text{Be}} \sim \frac{\langle\sigma v\rangle_{\text{bnd},7n_{^7\text{Be}}}}{H} Y_{\tilde{\tau}^-}, \quad (22)$$

where $\langle\sigma v\rangle_{\text{bnd},7} \sim 10^{-2}\text{GeV}^{-2}(T/30\text{keV})^{-1/2}(Z/4)^2 \times (A/7)^{-3/2}(E_{b^7\text{Be}}/1350\text{keV})$ is the thermally-averaged cross section times the relative velocity of the bound-state formation for ($^7\text{Be}\tilde{\tau}^-$) [15, 19]. Eq.(22) gives an approximate order of magnitude only under the condition of $Y_{\text{stau}} < Y_{^4\text{He}}$. We require $\Delta Y_{^7\text{Be}}$ to become $\sim \mathcal{O}(10^{-20})$ to reduce the abundance of ^7Be to fit the observational data. Then the abundance of $\tilde{\tau}^-$ should be the order of $\Delta Y_{^7\text{Be}}(\langle\sigma v\rangle_{\text{bnd},7n_{^7\text{Be}}}/H)^{-1} \sim \mathcal{O}(10^{-12})$ with $\langle\sigma v\rangle_{\text{bnd},7n_{^7\text{Be}}}/H \sim 10^{-8}$ at $T = 30$ keV. Because $\langle\sigma v\rangle_{\text{bnd},7n_{^7\text{Be}}}/H$ decreases as the cosmic temperature decreases ($\propto T^{1/2}$), the destruction is more effective just after the formation of the bound state. This validates that we have estimated (22) at 30 keV. Therefore the parameter region at around $Y_{\tilde{\tau}^-} \sim 10^{-12}$ and $\delta m \lesssim 130$ MeV is allowed by the observational ^7Li . Here $\delta m \lesssim 130$ MeV corresponds to $\tau_{\tilde{\tau}} \gtrsim 10^3$ s. The case for the destruction of ($^7\text{Li}\tilde{\tau}^-$) through the internal conversion is also similar to that of ($^7\text{Be}\tilde{\tau}^-$) [22, 26].

Further constraints come from the relic density of the dark matter, which can be stated in terms of the stau relic density. It is calculated as shown in Fig. 10 for the present values of parameters. Applying all the constraints, we are led to the allowed interval shown by the thick line in the figure.

4.3 Constraint on parameter space of stau

In the end, we show in Fig. 11 the parameter space in which the dark matter abundance and light elements abundances are consistent with the observations. Here, based on the discussion in previous subsection, we took $\delta m = 100$ MeV. Parameter region surrounded by black solid (blue dashed) line is allowed by the relic abundance of the dark matter from the WMAP observation at the 3σ (2σ) level [74], which corresponds to $0.0913 \leq \Omega_{\text{DM}}h^2 \leq 0.1285$ ($0.0963 \leq \Omega_{\text{DM}}h^2 \leq 0.1213$). Red crisscross points show the parameters which are consistent with the observational abundances for the light elements including ^7Li , where the observational ^7Li abundance is given in Ref. [2].

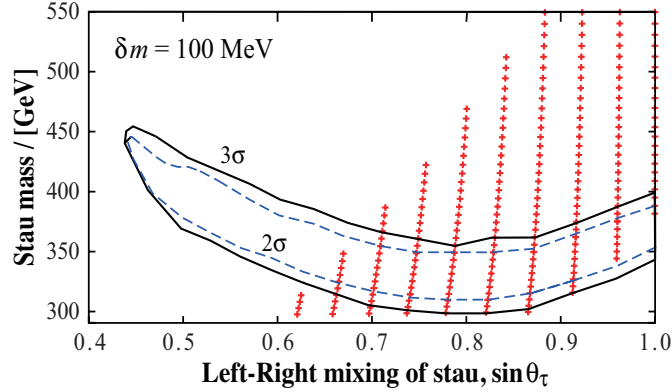


Figure 11: Parameter space of the stau for the observational abundances of the dark matter and that of the light elements [50]. The region surrounded by black solid (blue dashed) line shows the allowed region from the WMAP observation at the 3σ (2σ) level [74]. Red crisscross points show the parameters which is consistent with observational abundances for the light elements including ${}^7\text{Li}$ at 3σ level.

The abundance of the light elements constrains the parameter space due to the following reasons. First, the region where the stau mass is less than 300 GeV is excluded since the relic density becomes too small to destruct ${}^7\text{Li}$ sufficiently. Next, the top-left region of the figure is excluded since the lifetime of stau becomes too long and hence overproduces ${}^6\text{Li}$ through the catalyzed fusion [14]. The stau lifetime becomes longer as its mass becomes heavier [49]. On the other hand, the lifetime becomes shorter as the left-right mixing angle increases in the present parameter space [49]. As a result, the allowed region is obtained as shown by the red crisscrosses in Fig. 11.

The black solid curve and the blue dashed curve are the constraints from the relic abundance of the dark matter as discussed in the previous section. Note that the relic abundance is not so sensitive to the mass difference δm for $\delta m \ll m_{\tilde{\chi}}$. Combination of the constraints on the abundance of the light elements and of the dark matter strongly restricts the allowed region and leads to $\delta m \simeq 100 \text{ MeV}$, $m_{\tilde{\tau}} = (300 - 400) \text{ GeV}$, and $\sin \theta_{\tau} = (0.65 - 1)$. In Fig. 10, these parameter values correspond to the region which is surrounded by the curves of the thermal relic density (orange) and ${}^7\text{Li}/\text{H}$ with 3σ significance (purple). Our model can thus provide a nice probe to the mixing angle, which has few experimental signals, once the value of $m_{\tilde{\tau}}$ is determined.

5 Summary

In this review we expounded our idea to fit the primordial abundance of ${}^7\text{Li}$ to the observed value. We extend the SM to the supersymmetric SM (SSM). To explain the bino-like neutralino dark matter abundance with the coannihilation mechanism in the SSM, we have a long-lived scalar particle, stau. It can be so long-lived that it affects the BBN prediction. With appropriate parameters we can nicely fit the abundances both of ${}^7\text{Li}$ and the neutralino dark matter to the observed ones.

The key property is the small mass difference between the stau and the neutralino dark matter. It gives the following important features:

- (1) Very long life time of $\mathcal{O}(1000)\text{s}$ since the phase space is quite narrow and the open decay channel is only the 4 body decay (in Fig. 1 (c))
- (2) The stau in $({}^7\text{Be} \tilde{\tau}^-)$ very efficiently destructs ${}^7\text{Be}$, because the phase space becomes much wider in the bound state than that of the free stau decay. This is shown in Fig. 4. Comparing it with the Fig. 1 (b), it is understood as the opening of the threshold of the 3 body decay. Therefore the time scale of the destruction is of order 1 s or less.

These two features are available only in the case where the stau longevity is ensured by small mass difference, not in the case where the origin of the longevity is Planck suppressed coupling.

With such a stau we have to consider the following three processes in addition to the standard processes in the SBBN:

- (a) The destruction process of ${}^7\text{Be}$ (and ${}^7\text{Li}$) in the bound state with the stau (Sec. 3.1). It is often called “internal conversion”. This is important to reduce the primordial ${}^7\text{Li}$ abundance. More reactions make the prediction better.
- (b) The ${}^4\text{He}$ spallation processes in the bound state $({}^4\text{He} \tilde{\tau})$ (Sec. 3.2). These processes give extra light elements such as D, ${}^3\text{He}$. Less reactions are better. To evade the over-productions of light elements, the stau must not be long-lived so that it decays before $({}^4\text{He} \tilde{\tau}^-)$ is formed or δm must be large enough as shown in Fig. 8.
- (c) The ${}^6\text{Li}$ production process called catalyzed fusion ((8) in Sec. 3.2). If we take the ${}^6\text{Li}$ problem seriously, appropriate reaction rate of the catalyzed fusion would be needed. From this requirement we can pin down the parameter space if necessary.

We also evaluate the stau number density at the BBN era which is important and necessary to solve the Boltzmann equations of nucleosynthesis chain. Larger stau density makes the ${}^7\text{Li}$ abundance lower, and the larger

stau density is obtained for smaller mass difference of the stau and the neutralino.

Again we emphasize that the first two processes (a) and (b) are specific to our scenario, or more exactly to the small mass difference scenario. On the contrary the third process (c) can happen in all scenarios with long-lived charged massive particles.

As long as tau flavor is conserved exactly all the rate for the processes (a)-(c) and the stau number density are the function of only the mass difference δm eventually. In other words the prediction depends almost only on the mass difference.

Including all the processes we calculated the primordial abundance and we showed that we possibly have the solution to the ${}^7\text{Li}$ problem under the assumption of lepton flavor conservation.

The upper bound on δm is mainly determined by the requirement that the stau be long-lived enough to be relevant with the nucleosynthesis chain reactions. The lower bound also determined by the requirement that the stau be not too long-lived so that it would not destruct ${}^4\text{He}$ so much. Thus, in turn, to solve the ${}^7\text{Li}$ problem, we have very narrow allowed region for the parameter space. It gives a very precise prediction for particle physics like a collider phenomenology.

Before concluding the review we give a comment on the case that there is lepton flavor violation [51]. Including this we can relax the constraint on δm and we have a room to produce ${}^6\text{Li}$ appropriately by the catalyzed fusion. In this cases, for example, stau mixes with scalar electron,

$$\tilde{\tau} \rightarrow \tilde{l} = \tilde{\tau} + c_e \tilde{e}, \quad (23)$$

where \tilde{l} is a slepton, and c_e denotes a tiny mixing parameter with the selectron. The slepton can decay into a neutralino and an electron,

$$\tilde{l} \rightarrow \tilde{\chi}_1^0 + e. \quad (24)$$

Therefore the lifetime of the slepton will depend on not only δm but also c_e . The mixing parameter c_e must be very small, of $\mathcal{O}(10^{-10})$, so that the stau still be long-lived. With this degree of freedom we have a wider room for δm . The over-production of D and ${}^3\text{He}$ by the ${}^4\text{He}$ spallation processes (b) can be suppressed since δm can be very small. Therefore we would not have any constraint from this process as long as it is small enough.

On the contrary due to the smallness of c_e , the efficiency of the internal conversion process (a) still depends only on δm . The rate of the process is still rapid even if $\delta m \sim 30 \text{ MeV}$ as shown in Fig. 5.

By combining the smallness of δm and c_e , we get an allowed region (white) as shown in Fig. 12 where $c_e = 5 \times 10^{-11}$. Not only the ${}^7\text{Li}$ problem is solved within 3 (and almost 2) σ level, but also there is the “allowed” region for the ${}^6\text{Li}$ problem. If we do not take the ${}^6\text{Li}$ problem seriously,

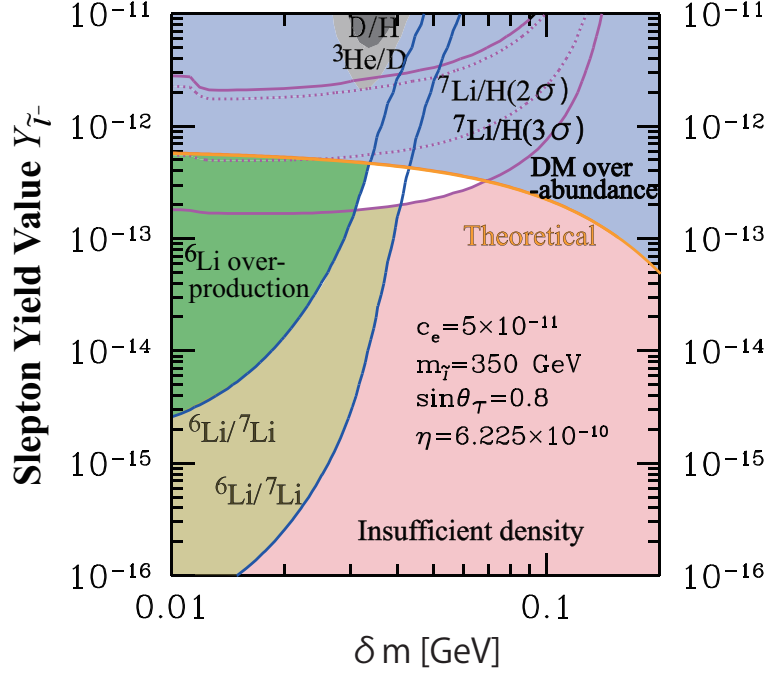


Figure 12: Allowed regions by observational light element abundances in δm - $Y_{\tilde{l}^-}$ planes in cases of $c_e = 5 \times 10^{-11}$ [51]. The lines of the constraints are plotted for D/H (dark grey), $^3\text{He}/\text{D}$ (light grey), and $^6\text{Li}/^7\text{Li}$ (blue curves) at 2σ . An exception is $^7\text{Li}/\text{H}$ (purple lines) whose constraints are denoted by both dotted lines at 2σ , and solid lines at 3σ . The theoretical curve of the slepton density is plotted as a thick solid (orange) line.

from its abundance all the right region of ^6Li over-production is the allowed region for the ^6Li abundance. If we take it seriously, the white band within two lines indicated $^6\text{Li}/^7\text{Li}$ is the allowed region and in near future once the ^6Li abundance is measured definitely we can pin down the allowed region within the white band. Thus, in this case both the ^6Li and the ^7Li problems are solved.

To conclude our review, we emphasize that we did not introduce any artificial particles. We employed the most extensively studied physics beyond the SM, that is, SSM. Within this theory we showed that the lithium problem(s) can be solved. We use the parameter which is required not by the lithium problem but by the explanation for dark matter abundance. In this sense our solution is very excellent!

Acknowledgments

This work is supported in part by the Grant-in-Aid for the Ministry of Education, Culture, Sports, Science, and Technology, Government of Japan, No. 25105009 (J.S.), No. 25003345 (Y.M.) and No. 15K17654 (T.S.).

References

- [1] F. Spite and M. Spite, *Astron. Astrophys.* **115**, 357 (1982).
- [2] J. Melendez and I. Ramirez, *Astrophys. J.* **615**, L33 (2004), [arXiv:astro-ph/0409383](#) [astro-ph].
- [3] P. Bonifacio *et al.*, *Astron. Astrophys.* **462**, 851 (2007), [arXiv:astro-ph/0610245](#) [astro-ph].
- [4] L. Monaco, P. Bonifacio, L. Sbordone, S. Villanova and E. Pancino, *Astron. Astrophys.* **519**, L3 (2010), [arXiv:1008.1817](#) [astro-ph.GA].
- [5] L. Monaco, S. Villanova, P. Bonifacio, E. Caffau, D. Geisler, G. Marconi, Y. Momany and H. G. Ludwig, *Astron. Astrophys.* **539**, A157 (2012), [arXiv:1108.0138](#) [astro-ph.SR].
- [6] W. Aoki, H. Ito and A. Tajitsu (2012), [arXiv:1204.3952](#) [astro-ph.SR].
- [7] M. A, S. M, B. P, M. L and V. S, *Mon. Not. Roy. Astron. Soc.* **444**, 1812 (2014), [arXiv:1407.7596](#) [astro-ph].
- [8] A. Coc, S. Goriely, Y. Xu, M. Saimpert and E. Vangioni, *Astrophys. J.* **744**, 158 (2012), [arXiv:1107.1117](#) [astro-ph.CO].
- [9] R. H. Cyburt, B. D. Fields and K. A. Olive, *JCAP* **0811**, 012 (2008), [arXiv:0808.2818](#) [astro-ph].
- [10] M. Asplund, D. L. Lambert, P. E. Nissen, F. Primas and V. V. Smith, *Astrophys. J.* **644**, 229 (2006), [arXiv:astro-ph/0510636](#) [astro-ph].
- [11] K. Lind, J. Melendez, M. Asplund, R. Collet and Z. Magic, *Astron. Astrophys.* **554**, A96 (2013), [arXiv:1305.6564](#) [astro-ph.SR].
- [12] O. Richard, G. Michaud and J. Richer, *Astrophys. J.* **619**, 538 (2005), [arXiv:astro-ph/0409672](#) [astro-ph].
- [13] M. Yu. Khlopov and A. D. Linde, *Phys. Lett.* **B138**, 265 (1984).
- [14] M. Pospelov, *Phys. Rev. Lett.* **98**, 231301 (2007), [arXiv:hep-ph/0605215](#) [hep-ph].

- [15] K. Kohri and F. Takayama, *Phys. Rev.* **D76**, 063507 (2007), [arXiv:hep-ph/0605243](#) [hep-ph].
- [16] M. Kaplinghat and A. Rajaraman, *Phys. Rev.* **D74**, 103004 (2006), [arXiv:astro-ph/0606209](#) [astro-ph].
- [17] R. H. Cyburt, J. R. Ellis, B. D. Fields, K. A. Olive and V. C. Spanos, *JCAP* **0611**, 014 (2006), [arXiv:astro-ph/0608562](#) [astro-ph].
- [18] F. D. Steffen, *AIP Conf. Proc.* **903**, 595 (2007), [arXiv:hep-ph/0611027](#) [hep-ph], [,595(2006)].
- [19] C. Bird, K. Koopmans and M. Pospelov, *Phys. Rev.* **D78**, 083010 (2008), [arXiv:hep-ph/0703096](#) [hep-ph].
- [20] M. Kawasaki, K. Kohri and T. Moroi, *Phys. Lett.* **B649**, 436 (2007), [arXiv:hep-ph/0703122](#) [hep-ph].
- [21] K. Hamaguchi, T. Hatsuda, M. Kamimura, Y. Kino and T. T. Yanagida, *Phys. Lett.* **B650**, 268 (2007), [arXiv:hep-ph/0702274](#) [HEP-PH].
- [22] T. Jittoh, K. Kohri, M. Koike, J. Sato, T. Shimomura and M. Yamanaka, *Phys. Rev.* **D76**, 125023 (2007), [arXiv:0704.2914](#) [hep-ph].
- [23] K. Jedamzik, *Phys. Rev.* **D77**, 063524 (2008), [arXiv:0707.2070](#) [astro-ph].
- [24] J. Pradler and F. D. Steffen, *Phys. Lett.* **B666**, 181 (2008), [arXiv:0710.2213](#) [hep-ph].
- [25] M. Kawasaki, K. Kohri, T. Moroi and A. Yotsuyanagi, *Phys. Rev.* **D78**, 065011 (2008), [arXiv:0804.3745](#) [hep-ph].
- [26] T. Jittoh, K. Kohri, M. Koike, J. Sato, T. Shimomura and M. Yamanaka, *Phys. Rev.* **D78**, 055007 (2008), [arXiv:0805.3389](#) [hep-ph].
- [27] M. Pospelov, J. Pradler and F. D. Steffen, *JCAP* **0811**, 020 (2008), [arXiv:0807.4287](#) [hep-ph].
- [28] M. Kamimura, Y. Kino and E. Hiyama, *Prog. Theor. Phys.* **121**, 1059 (2009), [arXiv:0809.4772](#) [nucl-th].
- [29] M. Kusakabe, T. Kajino, T. Yoshida, T. Shima, Y. Nagai and T. Kii, *Phys. Rev.* **D79**, 123513 (2009), [arXiv:0806.4040](#) [astro-ph].
- [30] S. Bailly, K. Jedamzik and G. Moulta, *Phys. Rev.* **D80**, 063509 (2009), [arXiv:0812.0788](#) [hep-ph].

- [31] S. Bailly, K.-Y. Choi, K. Jedamzik and L. Roszkowski, *JHEP* **05**, 103 (2009), [arXiv:0903.3974 \[hep-ph\]](#).
- [32] M. Kusakabe, T. Kajino, T. Yoshida and G. J. Mathews, *Phys. Rev.* **D81**, 083521 (2010), [arXiv:1001.1410 \[astro-ph.CO\]](#).
- [33] T. Jittoh, K. Kohri, M. Koike, J. Sato, K. Sugai, M. Yamanaka and K. Yazaki, *Phys. Rev.* **D84**, 035008 (2011), [arXiv:1105.1431 \[hep-ph\]](#).
- [34] R. H. Cyburt, J. Ellis, B. D. Fields, F. Luo, K. A. Olive and V. C. Spanos, *JCAP* **1212**, 037 (2012), [arXiv:1209.1347 \[astro-ph.CO\]](#).
- [35] M. Kusakabe, K. S. Kim, M.-K. Cheoun, T. Kajino and Y. Kino, *Phys. Rev.* **D88**, 063514 (2013), [arXiv:1305.6155 \[astro-ph.CO\]](#), [Erratum: *Phys. Rev.* **D88**, no.8, 089904(2013)].
- [36] ATLAS Collaboration, G. Aad *et al.*, *Phys. Lett.* **B716**, 1 (2012), [arXiv:1207.7214 \[hep-ex\]](#).
- [37] CMS Collaboration, S. Chatrchyan *et al.*, *Phys. Lett.* **B716**, 30 (2012), [arXiv:1207.7235 \[hep-ex\]](#).
- [38] WMAP Collaboration, C. L. Bennett *et al.*, *Astrophys. J. Suppl.* **208**, 20 (2013), [arXiv:1212.5225 \[astro-ph.CO\]](#).
- [39] Planck Collaboration, P. A. R. Ade *et al.*, *Astron. Astrophys.* **571**, A16 (2014), [arXiv:1303.5076 \[astro-ph.CO\]](#).
- [40] L. Bergstrom, *Rept. Prog. Phys.* **63**, 793 (2000), [arXiv:hep-ph/0002126 \[hep-ph\]](#).
- [41] C. Munoz, *Int. J. Mod. Phys.* **A19**, 3093 (2004), [arXiv:hep-ph/0309346 \[hep-ph\]](#).
- [42] G. Bertone, D. Hooper and J. Silk, *Phys. Rept.* **405**, 279 (2005), [arXiv:hep-ph/0404175 \[hep-ph\]](#).
- [43] J. L. Feng, *Ann. Rev. Astron. Astrophys.* **48**, 495 (2010), [arXiv:1003.0904 \[astro-ph.CO\]](#).
- [44] H. Goldberg, *Phys. Rev. Lett.* **50**, 1419 (1983), [Erratum: *Phys. Rev. Lett.* **103**, 099905(2009)].
- [45] J. R. Ellis, J. S. Hagelin, D. V. Nanopoulos, K. A. Olive and M. Srednicki, *Nucl. Phys.* **B238**, 453 (1984).
- [46] K. Griest and D. Seckel, *Phys. Rev.* **D43**, 3191 (1991).

- [47] J. R. Ellis, T. Falk, K. A. Olive and M. Srednicki, *Astropart. Phys.* **13**, 181 (2000), [arXiv:hep-ph/9905481 \[hep-ph\]](#), [Erratum: *Astropart. Phys.*15,413(2001)].
- [48] S. Profumo, K. Sigurdson, P. Ullio and M. Kamionkowski, *Phys. Rev.* **D71**, 023518 (2005), [arXiv:astro-ph/0410714 \[astro-ph\]](#).
- [49] T. Jittoh, J. Sato, T. Shimomura and M. Yamanaka, *Phys. Rev.* **D73**, 055009 (2006), [arXiv:hep-ph/0512197 \[hep-ph\]](#), [Erratum: *Phys. Rev.*D87,no.1,019901(2013)].
- [50] T. Jittoh, K. Kohri, M. Koike, J. Sato, T. Shimomura and M. Yamanaka, *Phys. Rev.* **D82**, 115030 (2010), [arXiv:1001.1217 \[hep-ph\]](#).
- [51] K. Kohri, S. Ohta, J. Sato, T. Shimomura and M. Yamanaka, *Phys. Rev.* **D86**, 095024 (2012), [arXiv:1208.5533 \[hep-ph\]](#).
- [52] Y. Konishi, S. Ohta, J. Sato, T. Shimomura, K. Sugai and M. Yamanaka, *Phys. Rev.* **D89**, 075006 (2014), [arXiv:1309.2067 \[hep-ph\]](#).
- [53] K. Kohri, M. Koike, Y. Konishi, S. Ohta, J. Sato, T. Shimomura, K. Sugai and M. Yamanaka, *Phys. Rev.* **D90**, 035003 (2014), [arXiv:1403.1561 \[hep-ph\]](#).
- [54] ATLAS Collaboration, G. Aad *et al.* (2015), [arXiv:1508.06608 \[hep-ex\]](#).
- [55] J. R. Ellis, T. Falk and K. A. Olive, *Phys. Lett.* **B444**, 367 (1998), [arXiv:hep-ph/9810360 \[hep-ph\]](#).
- [56] J. Edsjo, M. Schelke, P. Ullio and P. Gondolo, *JCAP* **0304**, 001 (2003), [arXiv:hep-ph/0301106 \[hep-ph\]](#).
- [57] L. Aparicio, D. G. Cerdeno and L. E. Ibanez, *JHEP* **04**, 126 (2012), [arXiv:1202.0822 \[hep-ph\]](#).
- [58] M. Citron, J. Ellis, F. Luo, J. Marrouche, K. A. Olive and K. J. de Vries, *Phys. Rev.* **D87**, 036012 (2013), [arXiv:1212.2886 \[hep-ph\]](#).
- [59] S. Kaneko, J. Sato, T. Shimomura, O. Vives and M. Yamanaka, *Phys. Rev.* **D87**, 039904 (2013), [arXiv:0811.0703 \[hep-ph\]](#), [Erratum: *Phys. Rev.*D87,no.3,039904(2013)].
- [60] J. Heisig and J. Kersten, *Phys. Rev.* **D84**, 115009 (2011), [arXiv:1106.0764 \[hep-ph\]](#).
- [61] T. Ito, K. Nakaji and S. Shirai, *Phys. Lett.* **B706**, 314 (2012), [arXiv:1104.2101 \[hep-ph\]](#).

- [62] K. Hagiwara, T. Li, K. Mawatari and J. Nakamura, *Eur. Phys. J.* **C73**, 2489 (2013), [arXiv:1212.6247 \[hep-ph\]](#).
- [63] MoEDAL Collaboration, B. Acharya *et al.*, *Int. J. Mod. Phys.* **A29**, 1430050 (2014), [arXiv:1405.7662 \[hep-ph\]](#).
- [64] N. Desai, J. Ellis, F. Luo and J. Marrouche, *Phys. Rev.* **D90**, 055031 (2014), [arXiv:1404.5061 \[hep-ph\]](#).
- [65] J. Heisig, A. Lessa and L. Quertenmont (2015), [arXiv:1509.00473 \[hep-ph\]](#).
- [66] C. Angulo *et al.*, *Nucl. Phys.* **A656**, 3 (1999).
- [67] D. Borisyuk, *Nucl. Phys.* **A843**, 59 (2010), [arXiv:0911.4091 \[hep-ph\]](#).
- [68] P. J. Mohr, B. N. Taylor and D. B. Newell, *Rev. Mod. Phys.* **80**, 633 (2008), [arXiv:0801.0028 \[physics.atom-ph\]](#).
- [69] R. B. Firestone, *John Wiley and Sons Inc, New York* (1999).
- [70] G. Kubon *et al.*, *Phys. Lett.* **B524**, 26 (2002), [arXiv:nucl-ex/0107016 \[nucl-ex\]](#).
- [71] C. W. Wong, *Int. J. Mod. Phys.* **E3**, 821 (1994).
- [72] M. Yoshitake *et al.*
- [73] P. Egelhof, *Prog. Part. Nucl. Phys.* **46**, 307 (2001).
- [74] WMAP Collaboration, J. Dunkley *et al.*, *Astrophys. J. Suppl.* **180**, 306 (2009), [arXiv:0803.0586 \[astro-ph\]](#).
- [75] T. Falk, K. A. Olive and M. Srednicki, *Phys. Lett.* **B339**, 248 (1994), [arXiv:hep-ph/9409270 \[hep-ph\]](#).
- [76] E. W. Kolb and M. S. Turner, *The Early Universe, Addison-Wesley, Redwood City, 1990*.
- [77] WMAP Collaboration, E. Komatsu *et al.*, *Astrophys. J. Suppl.* **192**, 18 (2011), [arXiv:1001.4538 \[astro-ph.CO\]](#).
- [78] S. G. Ryan, T. C. Beers, K. A. Olive, B. D. Fields and J. E. Norris, *Astrophys. J.* **530**, L57 (2000).
- [79] W. Aoki, P. S. Barklem, T. C. Beers, N. Christlieb, S. Inoue, A. E. G. Perez, J. E. Norris and D. Carollo, *Astrophys. J.* **698**, 1803 (2009), [arXiv:0904.1448 \[astro-ph.SR\]](#).

- [80] M. Pettini, B. J. Zych, M. T. Murphy, A. Lewis and C. C. Steidel, *Mon. Not. Roy. Astron. Soc.* **391**, 1499 (2008), [arXiv:0805.0594 \[astro-ph\]](#).
- [81] J. Geiss and G. Gloeckler, *Space Science Reviews* **106**, 3 (2003).
- [82] K. Jedamzik, *Phys. Rev.* **D70**, 063524 (2004), [arXiv:astro-ph/0402344 \[astro-ph\]](#).
- [83] M. Pospelov and J. Pradler, *Phys. Rev.* **D82**, 103514 (2010), [arXiv:1006.4172 \[hep-ph\]](#).
- [84] M. Kawasaki and M. Kusakabe, *Phys. Rev.* **D83**, 055011 (2011), [arXiv:1012.0435 \[hep-ph\]](#).
- [85] O. Erken, P. Sikivie, H. Tam and Q. Yang, *Phys. Rev. Lett.* **108**, 061304 (2012), [arXiv:1104.4507 \[astro-ph.CO\]](#).
- [86] J. Hisano, M. Kawasaki, K. Kohri, T. Moroi and K. Nakayama, *Phys. Rev.* **D79**, 083522 (2009), [arXiv:0901.3582 \[hep-ph\]](#).